Published in final edited form as:

Sci Signal. ; 7(357): ra121. doi:10.1126/scisignal.aaa1877.

Systematic identification of signaling pathways with potential to confer anticancer drug resistance

Colin A. Martz[1,†], **Kathleen A. Ottina**[2,3,†], **Katherine R. Singleton**[1,†], **Jeff S. Jasper**[1], **Suzanne E. Wardell**[1], **Ashley Peraza-Penton**[1], **Grace R. Anderson**[1], **Peter S. Winter**[1], **Tim Wang**[2,3,4], **Holly M. Alley**[1], **Lawrence N. Kwong**[5], **Zachary A. Cooper**[5], **Michael Tetzlaff**[5], **Pei-Ling Chen**[5], **Jeffrey C. Rathmell**[1], **Keith T. Flaherty**[6], **Jennifer A. Wargo**[5], **Donald P. McDonnell**[1], **David M. Sabatini**[2,3,4,*], and **Kris C. Wood**[1,*]

[1]Department of Pharmacology and Cancer Biology, Duke University, 450 Research Drive, Durham, NC 27710, USA

[2]Whitehead Institute for Biomedical Research, 9 Cambridge Center, Cambridge, MA 02142, USA

[3]Howard Hughes Medical Institute, Department of Biology, Massachusetts Institute of Technology, 77 Massachusetts Avenue, Cambridge, MA 02139, USA

[4]Broad Institute, 7 Cambridge Center, Cambridge, MA 02142, USA

[5]University of Texas M.D. Anderson Cancer Center, 1515 Holcombe Boulevard, Houston, TX 77030, USA

[6]Massachusetts General Hospital Cancer Center, 55 Fruit St, Boston, MA 02114

Abstract

Cancer cells can activate diverse signaling pathways to evade the cytotoxic action of drugs. We created and screened a library of barcoded pathway-activating mutant cDNAs to identify those that enhanced the survival of cancer cells in the presence of 13 clinically relevant, targeted therapies. We found that activation of the RAS– MAPK (mitogen-activated protein kinase), Notch1, PI3K (phosphoinositide 3-kinase)–mTOR (mechanistic target of rapamycin), and ER (estrogen receptor) signaling pathways often conferred resistance to this selection of drugs. Activation of the Notch1 pathway promoted acquired resistance to tamoxifen (an ER-targeted therapy) in serially-passaged breast cancer xenografts in mice, and treating mice with a γ-secretase

*Corresponding authors: sabatini@wi.mit.edu (D.M.S.), kris.wood@duke.edu (K.C.W.).
†These authors, listed alphabetically, contributed equally to this work.

Author contributions: K.C.W., K.A.O., T.W., and D.M.S. designed and created the barcoded screening library. K.C.W., K.A.O., and C.A.M. performed drug resistance screens. K.C.W. and T.W. analyzed screening data. K.R.S., K.C.W., C.A.M., G.R.A., P.S.W., and A.P.P. performed follow-up experiments on Notch1 in breast cancer and melanoma as well as pathway co-inhibition studies. J.S.J. and D.P.M. performed computational analyses of Notch1 pathway activation in breast cancer patients. S.E.W. planned, directed, and conducted animal experiments with assistance from H.M.A. J.A.W. and K.T.F. provided matched pretreatment and progression-stage melanoma patient samples and L.N.K., Z.A.C., M.T., and P.-L. C. analyzed these tumors for mutations in candidate resistance genes and expression of markers of interest by immunohistochemistry. All authors contributed to the design of experiments and analysis of results. K.C.W. wrote the manuscript, and all authors provided editorial input.

Competing financial interests: K.A.O., T.W., D.M.S., and K.C.W. are inventors on a United States patent application describing the barcoded pathway-centric screening technology. The authors declare no competing financial interests.

Data and materials availability: The screen data can be accessed from table S3 and the Wood laboratory website (http://wood.duhs.duke.edu/publications/index.html).

inhibitor to inhibit Notch signaling restored tamoxifen sensitivity. Markers of Notch1 activity in tumor tissue correlated with resistance to tamoxifen in breast cancer patients. Similarly, activation of Notch1 signaling promoted acquired resistance to MAPK inhibitors in $BRAF^{V600E}$ melanoma cells in culture, and the abundance of Notch1 pathway markers were increased in tumors from a subset of melanoma patients. Thus, Notch1 signaling may be a therapeutic target in some drug-resistant breast cancers and melanomas. Additionally, multiple resistance pathways were activated in melanoma cell lines with intrinsic resistance to MAPK inhibitors, and simultaneous inhibition of these pathways synergistically induced drug sensitivity. These data illustrate the potential for systematic identification of the signaling pathways controlling drug resistance that could inform clinical strategies and drug development for multiple types of cancer. This approach may also be used to advance clinical options in other disease contexts.

Introduction

Clinical resistance to anticancer therapies is a persistent problem that can be caused by genetic or epigenetic events occurring within cancer cells or by extracellular cues such as soluble factors or cell-cell contacts (1–6). Ultimately, these diverse events lead to the activation of growth and survival signaling pathways within cancer cells that enable them to survive otherwise lethal pharmacological insults (1–6). By blocking these drug resistance pathways, it may be possible to improve the efficacy and durability of anticancer drugs. However, for most drugs, the identities of potential resistance pathways are unknown (1).

We sought to develop a strategy to systematically identify the signaling pathways that, when activated, have the potential to confer resistance to therapeutic agents. If successful, such an effort could lead to a more complete understanding of the repertoire of signaling events that can render a cancer cell drug resistant, potentially resulting in improvements in our ability to (1) stratify patients into groups more and less likely to respond to therapy and (2) design multicomponent combination therapies that simultaneously act on cancer cell dependencies and resistance pathways.

Results

Screening to identify potential drug resistance pathways

With the objective of identifying key drug resistance pathways, we constructed a list of 17 signaling pathways that are frequently implicated in cancer cell proliferation, survival, differentiation, and apoptosis (7). For each pathway, a set of 1–3 mutant cDNAs were identified representing core nodes in each pathway that, when overexpressed, constitutively activated or inactivated the pathway (Fig. 1 and table S1). Pathway-activating mutants were used for those pathways that typically have tumor-promoting roles, whereas pathway-inhibiting mutants were used for those that have tumor-suppressive roles. All cDNAs in the collection were obtained, barcoded, and cloned into a PGK (phosphoglycerate kinase 1) promoter-driven lentiviral expression vector. Constructs were then fully sequenced (Data file S1) and produced as VSV-G pseudotyped lentiviruses (8), 86% of which (31/36) were functionally validated in cells by Western blotting, reporter gene assays, or immunofluorescence to ensure proper engagement of targeted pathways (table S1). Finally,

to screen library constructs for pathways with potential to confer resistance to anticancer drugs, we developed a modified, positive selection, pooled screening protocol with sequencing-based deconvolution that is analogous to those previously described (fig. S1) (9). The abundance of each cDNA in cells infected with the pooled library was assessed immediately after infection and again after 4 weeks in culture. In all cases, cDNA abundance was relatively stable (fig. S2).

To validate this screening approach, we first screened a *BRAF*-mutant melanoma cell line (UACC-62) to identify pathways of resistance to a MEK1/2 inhibitor (AZD6244). Resistance mechanisms to MAPK (mitogen-activated protein kinase) pathway inhibitors have been studied intensively in this setting. Our results corroborated the findings of these studies, showing that five major pathways are capable of conferring resistance to MEK1/2 inhibition in cultured cells. Three of these pathways – RAS– MAPK, PI3K –mTOR, and NF-κB – have been previously identified and are, in fact, frequently exploited by resistant tumors and cell lines thus far reported (10–13). Additionally, we found that two other previously unidentified pathways, those mediated by Notch1 and estrogen receptor (ER), were also capable of conferring resistance to MEK1/2 inhibition in this primary screen (Fig. S3).

On the strength of this technological validation, we then performed screens covering a total of 13 targeted therapies, most of which are either clinically approved, in clinical trials, or in late-stage preclinical development. Each drug was screened at two or three concentrations in 1 to 3 cell lines that had the appropriate drug-sensitizing genetic mutations and nanomolar drug sensitivity (Fig. 2A, and tables S2 and S3). Individual constructs whose expression conferred resistance to a given drug were identified as those yielding an Enrichment Score (the relative abundance of each construct in the presence of drug normalized to the same value in the absence of drug) of ≥1.5 and scoring in at least 2 of the 3 drug concentrations screened. This value was set because over 80% of constructs that scored at or above this level in pilot screens were successfully validated in subsequent eight-point GI50 (growth inhibition) assays. Twelve of 17 pathways scored as providing resistance to at least one drug, with the RAS–MAPK, Notch1, PI3K–mTOR, and ER pathways each scoring in over 30% of all screens (Fig. 2A and fig. S4A). Further, we also found that the cellular sensitivity to 11 of 13 drugs screened could be partially decreased by the activation of 5 or fewer pathways (fig. S4B). Finally, we noted that the manipulation of some pathways, such as the inhibition of apoptosis through the expression of dominant-negative caspases, rarely conferred resistance to targeted therapies in these assays, despite their demonstrable roles in modulating sensitivity to cytotoxic chemotherapeutics (fig. S5) (14).

A common theme in the targeted therapy of oncogene-driven cancers is the emergence of acquired resistance mediated by pathway reactivation, which can occur through copy number changes, alternative splicing events, mutations in members within the pathway, or second-site mutations in the drug target itself (1–4, 15). Thus, current efforts aim to inhibit pathway nodes downstream of the driving oncogene, on the assumption that pathway reactivation is more difficult to achieve following downstream pathway inhibition compared with upstream inhibition. This notion led to the use of MEK and ERK inhibitors to complement RAF inhibitors in the treatment of *BRAF*-mutant melanomas (10, 11, 16). By

combining resistance screening results with immunoblotting in melanoma cells that were treated with drugs targeting multiple nodes in the RAF–MEK–ERK pathway, we found that whereas cDNAs that reactivate the MAPK pathway at the level of ERK phosphorylation can drive potent resistance when the pathway is inhibited upstream of ERK, alternative resistance pathways that do not reactivate ERK phosphorylation dominate the resistance landscape when the pathway is inhibited "downstream" at the level of ERK (Fig. 2B and fig. S6). To our knowledge, these are the first evolutionary experiments demonstrating a shift in the resistance landscape based on the location of a pathway node targeted by a drug. These findings demonstrate that although downstream pathway inhibition may be an effective tactic for suppressing resistance that is driven by pathway reactivation, it is also likely to encourage the evolution of resistance driven by alternative pathways, a phenomenon that may have undesired consequences.

Notch1-driven resistance to targeted therapies in breast cancer cells

To identify findings from our screens with potential translational relevance, we first examined our data in breast cancer cells. We screened tamoxifen and fulvestrant (ER inhibitors) in MCF-7 estrogen-responsive (ER+) cells, lapatinib (HER2 inhibitor) in *HER2* amplified SkBr3 cells, and the PI3K-mTOR pathway inhibitors BKM-120 (PI3K inhibitor), MK-2206 (AKT inhibitor), Torin1 (mTORC1/2 inhibitor), and Rapamycin (mTORC1 inhibitor) in breast cancer cell lines with activating mutations in *PIK3CA* (BT-20, MDA-MB-453, and T47D) (Fig. 2A). The RAS–-MAPK and PI3K–mTOR pathways frequently scored as hits against these drugs, as expected (6, 17, 18). Additionally, the Notch1 pathway scored against these drugs, an observation that we validated through GI50 assays in cells that either expressed the Notch1 intracellular domain (N1 ICD, Fig. 3A) or were treated with the DSL peptide (residues 188–204 of the Notch ligand Jagged-1), a soluble Notch agonist (fig. S7) (19). Notch1-mediated resistance did not involve proximal reactivation of targeted signaling pathways, but was associated with the induction of canonical Hes and Hey family Notch1 target genes, the induction of a dedifferentiation process that resembled the epithelial-to-mesenchymal transition (EMT), and the acquisition of enhanced migration, sphere formation, and apoptosis resistance properties as well as cross-resistance to cytotoxic agents, like doxorubicin (Fig. 3, A and B; figs. S8 and S9) (7, 20). These findings are consistent with the established role of the Notch1 pathway in stimulating EMT in epithelial cells and its prior association with resistance to cytotoxic chemotherapies and targeted inhibitors of EGFR (epidermal growth factor receptor) and PI3K in epithelial cancer cells (21–24).

Resistance to endocrine therapy (such as tamoxifen) is a major clinical problem that eventually occurs in most patients with ER+ metastatic breast cancer (17). Given our finding that Notch1 can drive resistance to tamoxifen in cultured cells, and the fact that Notch1 and ER reciprocally regulate each other in ER+ cells (25), we reasoned that this pathway may play a role in acquired resistance. To test this hypothesis, we used a mouse model of tamoxifen resistance (TamR) in which MCF-7 xenografts acquired resistance through selective pressure induced by serial passaging in the presence of tamoxifen in vivo (26). In this model, as in patients with tamoxifen-resistant disease, tamoxifen exerts pronounced growth agonist activity to the tumors in mice. This model also retains sensitivity to

fulvestrant. The expression of *NOTCH1*, Notch1 target genes, and genes encoding mesenchymal markers were significantly increased in TamR tumors relative to tamoxifen-sensitive parental tumors (Fig. 3C and fig. S10), consistent with potential Notch1 pathway activation. Further, co-treatment of TamR tumors with tamoxifen and RO4929097, a γ-secretase inhibitor that blocks Notch1 signaling (27), blocked tamoxifen-stimulated growth in these tumors (Fig. 3D). Corroborating these data, we also found that in a meta-analysis of 458 women with ER+ breast cancer enrolled across multiple studies, Notch1 activation (evident as induction of a Notch1-associated gene expression signature) correlated with the acquisition of a dedifferentiated phenotype and loss of the beneficial effects of tamoxifen on distant recurrence free survival. This effect was specific to tamoxifen, as outcomes in women not treated with tamoxifen were not correlated with Notch1 activation (Fig. 3, E and F; fig. S11) (28–30). Together, these data suggest that Notch1 activation may drive resistance to tamoxifen in vivo and that patients with tamoxifen-resistant disease may benefit from combination therapy using γ-secretase inhibitors.

Notch1-driven resistance to targeted therapies in melanoma cells

In melanoma, we screened three inhibitors of the Ras-MAPK pathway: PLX-4720 (a RAF inhibitor), AZD6244 (a MEK1/2 inhibitor), VX-11E (an ERK-2 inhibitor), each in MAPK inhibitor-sensitive melanoma cell lines harboring activating mutations in *BRAF* (A375, Colo679, and UACC-62) (Fig. 2A). Consistent with our pilot screen involving AZD6244, these screens revealed that resistance can be driven by MAPK reactivation or compensatory activation of the PI3K–mTOR, NF-κB, Notch1, and ER pathways. Notch1 and ER signaling have not been previously implicated in MAPK inhibitor resistance in melanoma. GI50 assays revealed that Notch1 activation conferred robust GI50 shifts of 0.5–2 orders of magnitude in multiple cell lines treated with MAPK inhibitors (Fig. 4A), whereas ER activation conferred more modest GI50 shifts of 2.5–3-fold for the same drugs (fig. S12). Because of the strength of Notch1-mediated resistance, we chose to focus our follow-up efforts in melanoma primarily on this pathway. Analogous to our findings in breast cancer cells, expression of the N1-ICD increased the expression of Notch1 target genes and stimulated the dedifferentiation of melanoma cells, resulting in the loss of melanoma-specific antigens tyrosinase (TYR) and DCT (TRP-2) (31) and increased expression of markers associated with melanocyte dedifferentiation, such as NGFR and N-cadherin (32) (Fig. 4B and fig. S13). Furthermore, Notch1-activated cells exhibited increased migration, melanosphere formation, and viability and did not reactivate ERK activation (phosphorylation) in the presence of drug treatment, suggesting that the Notch1 pathway operates independently – or possibly downstream – of ERK and supports the maintenance of a dedifferentiated state (figs. S14 and S15).

To explore the potential role of Notch1 in the setting of acquired resistance, which occurs in most patients who initially respond to RAF and/or MEK inhibitor therapy, we first induced resistance to RAF, MEK, and ERK inhibitors in a panel of six cell lines by step-wise selection (33). In 7/18 (39%) of these derivatives, Notch1 knockdown by two independent shRNAs fully resensitized drug-resistant cells to MAPK inhibitors (Fig. 4C, fig. S16, and table S4). Eighty-four clonal derivatives of these lines were also established, 24 of which were resensitized to MAPK inhibitors by Notch1 knockdown (29%) (fig. S17). In cell lines

whose resistance appeared to be Notch1-dependent, resistance to MAPK inhibitors was associated with the increased expression of Notch1, Notch1 target genes, and markers of dedifferentiation, as well as the absence of ERK pathway reactivation (evident by the loss of ERK phosphorylation in the presence of MAPK pathway inhibitors) (Fig. 4D and fig. S17). To identify potential clinical correlates of these findings, we examined two independent cohorts of matched pretreatment/post-relapse tumor samples from *BRAF*-mutant melanoma patients. In each cohort, we searched for evidence of Notch1 activation in relapsed tumors that is consistent with the activation observed in engineered and evolved Notch1-activated cells: increased Notch1 and Notch1 target gene expression (>two-fold) with concomitant decreased expression of differentiation markers or increased expression of dedifferentiation markers. In cohort 1, we queried gene expression and targeted sequencing data from a published set of 29 matched pretreatment/post-relapse tumors from patients treated initially with the RAF inhibitors vemurafenib or dabrafenib (34). Fifteen of 29 relapsed tumors (52%) showed evidence of canonical acquired mutations in MAPK pathway genes (*NRAS*, *BRAF*, *MEK1*, and *MEK2*), and 1/29 had an activating mutation in *AKT1* (34). Twelve of 29 relapsed tumors (41%) lacked evidence of canonical MAPK or PI3K pathway alterations. Among this latter group, four (14% of total) exhibited expression patterns consistent with Notch1 activation (Fig. 4E and fig. S18). Additionally, one relapsed tumor exhibited evidence of coincident Notch1 activation and IGF-1R overexpression (Fig. S18). To verify these findings, we obtained a second, independent cohort of matched pretreatment/post-relapse samples from seven patients with acquired resistance to RAF or RAF+MEK inhibitor combinations. Consistent with cohort 1, three of seven (43%) relapsed tumors harbored acquired MAPK pathway alterations (*BRAF*, *MEK2*), 1/7 (14%) harbored a *PTEN* mutation, and 3/7 (43%) lacked canonical resistance alterations. Two of the tumors in the latter group (29% of total) exhibited Notch1 activation on relapse as judged by the criteria above, whereas none of the four tumors with MAPK/PI3K pathway alterations showed evidence of Notch1 activation (Fig. 4, F and G; fig. S19, and table S5). Together, these data demonstrate that Notch1 activation can drive acquired resistance to MAPK inhibitors in engineered and evolved cellular models and suggest that Notch1 signaling is likely to play a role in the minority of patients whose relapsed tumors lack conical MAPK or PI3K pathway-mediated resistance mechanisms. These findings are also consistent with emerging data suggesting that the Notch1 pathway promotes melanoma tumor growth and may act as an essential mediator of tumorigenesis downstream of *BRAF* (35, 36).

Finally, we sought to assess the potential relevance of our findings in the setting of intrinsic resistance to MAPK inhibitors, which occurs in 10 to 20% of *BRAF*-mutant melanoma patients (37). To assess whether Notch1 activation may be responsible for this phenomenon, we obtained eight *BRAF*-mutant melanoma cell lines and short-term cultures exhibiting intrinsic resistance to MAPK inhibitors (GI50 > 4 μM) through uncharacterized mechanisms (37, 38). Although these cultures exhibited higher expression of certain Notch1 target genes, lower expression of melanocyte differentiation markers, and higher expression of dedifferentiation markers than a reference cohort of MAPK inhibitor-sensitive cell lines (Colo679, UACC-62, and Malme3M) (Fig. 5A), knocking down Notch1 by two independent shRNAs only modestly sensitized six of eight of these cell lines to MAPK inhibitors (Fig. 5B). Thus, we concluded that although Notch1 appears to play a functional role in the

maintenance of intrinsic resistance in these cells, other factors are likely to contribute to this state as well. Given that our screening results suggested that the PI3K–mTOR, NF-κB, and ER pathways are also capable of driving resistance to MAPK pathway inhibitors, we hypothesized that full sensitization of intrinsically resistant cells may require simultaneous inhibition of more than one of these pathways. To test this hypothesis, we co-treated these cultures with the combination of an ER inhibitor (fulvestrant), a dual PI3K–mTOR inhibitor (BEZ-235), and shRNA against Notch1 (IKKα/β inhibitors for the NF-κB pathway had no effect on MAPK inhibitor sensitivity and were thus excluded). Remarkably, this combination converted all eight drug resistant cultures to a drug sensitive state, with submicromolar VX-11E GI50 values comparable to those typically found in drug-sensitive cell lines (Fig. 5C). Although this drug cocktail exerted background effects on cell growth rate (~50%), its effects on VX-11E sensitivity were nevertheless specific and not owing to a general “sick + sick” phenomenon, as (1) background toxicity was removed prior to GI50 analysis (refer to Methods), (2) numerous control drugs and drug combinations with similar overall toxicity had no effect on VX-11E sensitivity (fig. S20), and (3) the cocktail had only modest effects on VX-11E sensitivity in MAPK inhibitor-sensitive cell lines (Fig. 5C). Finally, by applying all possible combinations of resistance pathway inhibitors to each resistant culture, we were able to deconvolute the particular set of pathways maintaining the resistant state in that culture. Four of eight cultures showed evidence of resistance mediated by the combination of all three resistance pathways (ER, Notch1, and PI3K–mTOR); three of eight cultures relied only on the Notch1 and PI3K–mTOR pathways; and one culture (RPMI-7951) relied exclusively on the PI3K–mTOR pathway for the maintenance of its resistant state (Fig. 5D).

Discussion

By enabling the direct screening of signaling pathways instead of individual genes (8, 39), the methods described here may significantly accelerate the systematic mapping of pathways to the oncogenic phenotypes, such as drug resistance, which they control. In the future, these methods may be further improved by utilizing expression vectors that normalize transgene expression to physiological levels and mutants that reflect naturally-occurring mechanisms of pathway activation in human cancers, steps that may minimize the potential for non-physiological signaling effects. The lack of these features in the current screening library may explain, for example, why $HRAS^{G12V}$ scored more frequently in screens than $KRAS^{G12V}$ or why myr-*AKT1* scored more frequently than myr-*PIK3CA*. Further, although the pathway-activating library described here encompasses many of the pathways most frequently implicated in cancer physiology, it will be improved by the addition of constructs representing additional signaling nodes and biological pathways, a process that is currently underway.

In the area of drug resistance, our findings begin to reconcile two disparate notions of how this phenomenon may emerge: one based on reactivation of drug-inhibited signaling pathways and the other based on the reversion of cancer cells to a dedifferentiated state (1, 40). Our findings suggest that both may occur simultaneously, and that the latter, mediated by the Notch1 pathway, may be a particularly effective strategy for generating broad-spectrum resistance to drugs with varying mechanisms of action. Whereas the induction of

an EMT-like process has been described extensively as a mode of therapeutic resistance in epithelial cancers, these results provide evidence of an analogous, Notch1-driven process in melanoma that may also contribute to therapeutic resistance. The precise molecular mechanisms by which Notch1 is activated in tumors resistant to tamoxifen and MAPK inhibitors, the identification of biomarkers of Notch1-driven resistance, and clarification of the cellular mechanisms by which this pathway drives therapeutic resistance will each be important areas for future study. Finally, this work describes a straightforward approach for designing combinations of drugs that block or reverse resistance by simultaneously inhibiting multiple resistance pathways. Although such combinations may frequently require the use of three or more drugs in parallel, an abundance of clinical evidence suggests that multidrug therapies can sometimes be safely tolerated by patients (41–44).

Materials and Methods

Cell lines and drugs

A375, Colo679, UACC62, Malme3M, WM793, WM1716, WM1745, WM1930, and SkBr3 were grown in RPMI with 10% fetal bovine serum (FBS) and 1% penicillin/streptomycin. BT20, T47D, SkMel28, Lox IMVI, Hs294T, A2058, MCF7, MDA-MB-453, Kato III, NCI-H1703, 293T, and RPMI-7951 were grown in DMEM with 10% FBS and 1% penicillin/streptomycin. Ly.1 and DHL4 cells were grown in Iscove's modified DMEM supplemented with 10% FBS, HEPES, Glutamine, β-mercaptoethanol, and 1% penicillin/streptomycin. Malme3M, WM793, WM1716, WM1745, WM1930, SkMel28, Lox IMVI, Hs294T, A2058, and RPMI-7951 cells were obtained from Levi Garraway (Harvard University, Dana-Farber Cancer Institute). All other cell lines were purchased from American Type Culture Collection (ATCC). Drugs were purchased from Selleck Chemicals, ChemieTek, and Sigma-Aldrich. Torin1 was obtained from N. S. Gray (Harvard University, Dana-Farber Cancer Institute). DSL peptide was obtained from Anaspec.

Library construction and validation

cDNA templates obtained from sources listed in table S1 were barcoded and transferred into the Gateway system via PCR and recombinational cloning (8). Donor vector pDONR223 and destination/expression vector pcw107 were kindly donated by John Doench (Broad Institute) (fig. S21). A C-terminal V5 epitope tag was added to pcw107 to tag constructs lacking functionally validated N-terminal tags. Barcoded attB1 primers were generated containing a 4 nucleotide (nt) barcode assigned to individual constructs followed by a 14 nt common linker sequence containing a Kozak sequence and ~21 nt of the ORF (open reading frame) of interest. AttB2 primers were generated to contain the final 21 or 24 nt of the ORF depending on whether a C-terminal V5 tag was desired. In general, constructs already containing an N-terminal epitope tag were cloned without a C-terminal V5 tag. Constructs not containing an N-terminal epitope tag were cloned both with and without the C-terminal V5 tag, and both constructs were functionally validated. For details, refer to tables S1, S6, and S7. The PCR fragments were gel purified and used in the BP recombination reaction using BP clonase (Invitrogen) with pDONR223 to generate entry clones. Individual clones were sequence verified using primers M13-F and M13-R to ensure proper integration of the N-terminal barcode linker sequence and the presence/absence of the C-terminal stop codon

(table S7). Two of the constructs, SMO and LATS2, were further manipulated using Agilent's QuickChange II XL Site-Directed Mutagenesis kit and appropriate primers to generate the desired activating mutations (tables S1 and S7). Entry clones were then used in the LR recombination reaction using LR clonase (Invitrogen) with pcw107-V5 to obtain lentiviral expression clones. All expression clones were fully sequenced using primers PGK-F and WPRE-R and gene-specific internal sequencing primers as needed to verify the presence of the N-terminal barcode, the linker sequence, the desired activating mutations, and the presence or absence of the V5 tag (table S7).

Functional validation of library clones was performed as follows. First, expression clones were used to produce lentivirus particles by transfecting 293T cells using a three-plasmid system (expression clone + VSV-G + ∂VPR) as previously described (8). Each virus was titered via infection with limiting dilution in UACC-62 cells (8). ORF transgene expression was measured by western blot by probing for the epitope tag present in each construct in 293T cell lysates stably infected with each lentivirus. Pathway activation was assessed using the assays summarized in table S1 in 293T cells following infection and puromycin selection. All infections were performed by adding a 1:10–1:20 dilution of lentivirus to 293T cells in 6-well plates in the presence of 7.5 μg/ml polybrene. After virus addition, plates were centrifuged at 1200*g* for 1 hour at 37° C. Twenty-four hours after infection, puromycin (2 μg/ml) was added for selection and cells were incubated for 48 hours.

Primary screens

All pathway-activating constructs and controls (table S1) were produced in lentiviral form, individually titered, and pooled together in approximately equal representation. The mixed pool was aliquoted and stored at −80° C. Screens were performed by seeding each cell line at 500,000 cells/well in a single well of a 6-well plate. Twenty-four hours later, the cells were infected with the mixed virus pool at an MOI of 0.3 to ensure that most infected cells contained only a single viral integration. The lentiviral pool was added directly to cells in the presence of polybrene (7.5 μg/mL), then plates were centrifuged at 1200*g* for 1 hour at 37° C. Twenty-four hours after infection, media was replaced with puromycin (2 μg/ml) for selection. After 48h of selection, cells were split and divided into (typically) seven equal portions, one of which was frozen at −80° C (t=0 infected cell pool), and the other six were added to the wells of a 6-well plate. Twenty-four hours later, two to three of the wells received drugs at indicated doses (typically in the range of the drug's GI20-GI80) and the remaining three wells received vehicle (DMSO) only. Drugs and vehicle were refreshed every 3 days for 2 to 3 weeks, splitting (1:10) as necessary. After this culture period, all drug- and vehicle-treated samples were trypsinized and washed, and genomic DNA was isolated using the Qiagen DNeasy Blood and Tissue Kit.

Genomic DNA samples were prepared for Illumina Sequencing by PCR amplification of individual construct barcodes using a common P5 Illumina adapter primer (PGK-Illumina-F) and a unique P7 Illumina barcoded adapter primer (P7-Illumina–RIP-Index-X where X is a unique numerical identifier for each indexed primer) (table S7). Each drug- or vehicle-treated screen sample was associated with a unique P7-Illumina–RIP-Index-X primer to facilitate pooling of samples and sequencing in a single Illumina lane. The P5 primer targets

the PGK promoter upstream of the construct barcode and the P7-reverse index primers target the ATG of the ORF downstream of the construct barcode. P7-reverse index primers contain a 6 nt Index barcode and the reverse complement of the ATG plus 14 nt linker sequence just downstream of, but not including, the 4 nt construct barcode. When paired, these Illumina adapter primers generate a ~250 nt DNA fragment, a fraction of which was visualized on a 2% agarose gel. Band intensities, which are proportional to the amount of barcode DNA amplified from each sample, were quantified and a normalized sample pool containing all samples to be sequenced was submitted for Illumina sequencing. A custom designed Illumina Sequencing Primer (ISP) that targets the region of gDNA just upstream of the 4nt barcode was used, yielding 27 nt Illumina HiSeq reads with the following structure: 4 nt construct barcode + 17 nt linker sequence/ATG + 6 nt index barcode (table S7). Each sample was prepared with two different Illumina-P7-RIP-Index barcodes, generating technical replicates. Both technical replicates (i.e. a single sample whose barcodes were PCR amplified using two unique sets of primers) and biological replicates (i.e. two replicate vehicle-treated screen samples) yielded comparable data ($R^2 > 0.9$), and replicates were averaged in the data sets reported here.

Analysis of Illumina sequencing data proceeded as follows. First, the number reads associated with each unique sequence (4 nt construct barcode + 6 nt index barcode) were counted, and the fractional representation of each construct barcode in each screen was determined by normalizing the number of reads associated with that construct barcode to the total number of reads in that sample (that is, all samples containing the same index barcode). Next, fractional representation of each construct in technical replicates was averaged, and the fractional representation of each construct in three biological replicate, vehicle-treated samples was averaged. Finally, the fractional representation of each construct in drug-treated samples was normalized to the same quantity in vehicle-treated samples of the same cell line. Hits were identified as constructs selectively enriched in drug-treated samples relative to vehicle-treated samples. In order for a signaling pathway to be considered a resistance pathway for a given drug, we required that at least one activating construct for that pathway must confer >50% enrichment above controls and that it must score in two or more drug concentrations in primary screens.

Secondary GI50 assays

ORF- or shRNA-expressing lentiviruses were produced as previously described (13) and used to infect cells at a 1:10–1:20 dilution in 6-well plates in the presence of polybrene (7.5 μg/ml). After virus addition, plates were centrifuged at 1200*g* for 1 hour at 37° C. Twenty-four hours after infection, puromycin (2 μg/ml) was added for selection and cells were incubated for 48 hours. Cells were then trypsinized, counted, and seeded into 96-well plates at 5,000 cells/well. Twenty-four later, DMSO or concentrated serial dilutions of indicated drugs (in DMSO) were added to cells (1:1,000) to yield final drug concentrations of 100, 10, 1, 0.1, 0.01, 0.001, 0.0001, or 0.00001 μM. The Cell Titer Glo® luminescent viability assay (Promega) was used to measure cell viability 4 days after drug addition. Viability was calculated as the percentage of control (untreated cells) after background subtraction with a minimum of three replicates for each cell line/ORF (or shRNA)/drug/concentration. GI50 values were determined as the drug dose corresponding to half-maximal growth inhibition

(13). GI50 values for unmodified parental cells were determined using the protocol above by seeding cells directly into 96-well plates without the initial infection step. Similarly, GI50 values for parental cells treated with DSL peptide were determined using the protocol above by seeding cells directly into 96-well plates in media containing DSL peptide at the indicated concentrations.

qRT-PCR

RNA was extracted using QIAshredder Homogenizers and RNEasy Mini Kits according to the manufacturer's specifications (Qiagen, Germany). RNA purity as measured by A_{260}/A_{280} was confirmed upon quantification. cDNAs were synthesized using iScript™ cDNA Synthesis Kits with at least 1μg of RNA template as directed by the protocol provided by the manufacturer (Bio-Rad).

Quantitative real-time polymerase chain reactions (qRT-PCR) were carried out using iQ™ SYBR® Green Supermix and a CFX384 Touch™ Real-Time PCR Detection System according to the manufacturer's specifications (Bio-Rad, USA). PCR primers purchased from Integrated DNA Technologies and processed to 10μM working stocks for use in qPCR reactions (table S7). Average cycle threshold (C_t) values were calculated for each gene and the maximum C_t value was set at 40 cycles. C_t values were normalized to the reference genes GAPDH and β-actin and relative gene expression was determined using the $\Delta\Delta C_t$ method.

Xenograft tumor analyses

All procedures were approved by the Duke University Institute for Animal Care and Use Committee. Tamoxifen stimulated TamR tumors were initiated orthotopically by serial transfer into female NU/NU mice (~6 weeks age, Duke breeding colony). Briefly, ovariectomized recipient mice received no treatment or tamoxifen (tam) treatment via a timed release pellet (5 mg tamoxifen/60 days – Innovative Research of America) implanted subcutaneously. Two days later, TamR tumors (~0.8cm^3 volume) were sterilely excised from euthanized tam treated donor mice, diced to ~2mm^3 sections and implanted into the axial mammary gland of recipient mice under anesthesia (10g trochar). Tumor growth was measured three times weekly by caliper (tumor volume = $(A^2 \times B)/2$, where A is the longer axis). When tumor volume reached ~0.15cm^3 (~20 days), mice (n = 9–13) were randomized to vehicle or RO 4929097 treatment (10 mg/kg oral gavage in 0.1cc 1% hydroxypropyl cellulose/0.2% tween 80/2.5% DMSO). Tumor growth was monitored over 4 weeks of daily treatment.

Gene expression analysis

Survival analysis of Notch1 and Notch1 gene sets in breast cancer presented in Fig. 3e and 3f: A breast cancer metaset was compiled from 26 publicly available expression data sets comprising 4886 patients. Breast cancer data from GPL570 and GPL96 platforms were downloaded from GEO, normalized with fRMA and batch corrected using the COMBAT algorithm within R. Associated clinical features and patient response data were combined and tumor subtypes were called using the PAM50 algorithm. Gene expression was split into tertiles and only the low (1st tertile) and high (3rd tertile) categories are plotted. Survival

curves were generated using the survival package in R and all P-values were calculated using the log-rank method. Gene sets representing the Notch1 pathway and Notch1 target genes were downloaded from GSEA and the R package genefu was used to assign signature scores of each gene set to patients by mapping Affymetrix probes to entrez ids. Signature scores were then categorized into low and high groups for each treatment condition and plotted similarly as above. For Gene Set Enrichment Analysis, a ranked list of pairwise gene correlation of Notch1 and all other probesets on the HGU133A platform from Luminal B tumor samples were submitted to the GSEAPreranked tool for pathway enrichment. Metaplot (fig. S11A) was generated using Luminal B patients from the assembled breast cancer metaset in R with the rmeta and survcomp packages. Correlation matrix (fig. S11B) was clustered using Ward's method and visualized using the corrplot package in R.

Patient samples

Details on patient sample acquisition, quality control, total RNA extraction, cDNA preparation, and mRNA sequencing are described elsewhere (31). Immunohistochemistry on patient tumor samples was performed as follows: sections (5 μm) were deparaffinized in xylene, followed by serial hydration in 100%, 95%, 70%, and 50% ethanol, then dH_2O. Sections were then placed in sodium citrate buffer (10 mM, pH 6.0) and boiled in a pressure chamber at 95°C for 30 min, 90°C for 10 s, and then cooled to room temperature. Immunohistochemistry (IHC) was performed using an antibody to activated Notch1 (Abcam; ab8925; 1:100) at 4°C overnight, and the tissue sections were incubated with secondary antibody (Abcam ab64256) at room temperature for 30 min, then washed with TBST for 5 min three times. Immunoreactivity was detected using the Dako liquid DAB+ substrate chromogen system.

Small molecule sensitization assays

Sensitization assays using small molecule signaling pathway inhibitors were performed to assess the effect of resistance pathway inhibition on the sensitivities of drug resistant melanoma cell lines to VX-11E. VX-11E GI50 values for parental cell lines were determined as above with DMSO added to media at a 1:1000 dilution as a vehicle-only control. GI50 values for parental cell lines in the presence of inhibitors were obtained using a modified version of the GI50 protocol above, where pathway inhibitors were added to all wells containing VX-11E as well as one set of triplicate wells containing media only (pathway inhibitors were in DMSO at a 1:1000 dilution in media). As a reference, a second set of media-only wells contained no pathway inhibitors (media and DMSO only). By comparing the viability of cells in media-only wells to the viability of cells in wells containing media plus pathway inhibitors (no VX-11E), the toxicity of the inhibitors alone was ascertained. GI50 values were then determined as the VX-11E dose corresponding to half-maximal growth inhibition relative to the viability in inhibitor-only wells.

Immunoblotting

Immunoblotting was performed as previously described (13) and blots were probed with primary antibodies (1:1000 dilution) recognizing N-cadherin (BD Transduction), Vimentin (Cell Signaling), Slug (Cell Signaling), phosphorylated AKT (Thr^{308}, Cell Signaling), AKT (Cell Signaling), Tyrosinase (Santa Cruz Biotechnology), TRP-2 (Santa Cruz

Biotechnology), β-actin (Cell Signaling), Notch1 (Cell Signaling), phosphorylated ERK1/2 (Thr^{202}/Tyr^{204}, Cell Signaling), phosphorylated MEK1/2 (Ser^{217}/Ser^{221}, Cell Signaling), ERK1/2 (Cell Signaling), and Na/K ATPase (Cell Signaling).

Notch shRNAs

TRC shRNA clones for Notch1 were obtained from Sigma-Aldrich as glycerol stocks. They were prepared in lentiviral form and used to infect target cells via the procedures described above for ORF clones. shNotch1 #1 is TRCN0000350330 with target sequence CCGGGACATCACGGATCATAT and shNotch1 #2 is TRCN0000003360 with target sequence CGCTGCCTGGACAAGATCAAT.

In vitro adaptation of MAPK inhibitor-resistant cells

Cell lines resistant to PLX4720, AZD6244 or VX-11E were generated by two methods as previously described (45). Briefly, cells were either cultured in gradually increasing concentrations of the inhibitor starting with a concentration of 1 nM [slow method, denoted with (S)] or 3×10^6 cells were treated with 3 μM inhibitor and resistant clones were cultured [fast method, denoted with (F)]. Cell lines were deemed resistant when they could be consistently cultured in medium containing 3 μM inhibitor. Parental control cell lines were cultured concurrently with the resistant cell lines in growth media containing DMSO.

Clonogenic growth assay

To measure the effect of inhibitors and shRNA-mediated knockdown on cell growth, cells were seeded at 10,000 cells per well in six-well tissue culture plates in complete media. After 24 hours, cells were infected with 1×10^5 infectious units (IFUs) per well of viral media containing shRNA vectors targeted to either GFP or Notch1 and polybrene (8 μg/mL). Twelve hours post-infection, cells were treated with growth media containing inhibitors as indicated and puromycin (2 μg/mL). Fresh media and inhibitors were added every seven days and the assays were cultured for 10–20 days. Plates were then rinsed with PBS and fixed and stained with 0.5% (wt/vol) crystal violet in 6.0% (vol/vol) gluteraldehyde solution (ThermoFisher Scientifics) for 30 min at room temperature. Plates were rinsed in distilled H_2O and scanned. The ImageJ software program and the ColonyArea plugin (46) were used to quantify colony area as a percentage of the well covered.

Sphere formation assay

The ability of pathway activated cells to form spheres on low-attachment plates was analyzed using previously described assays (47, 48). A single cell suspension was created by passing cell suspensions through a 70 μm strainer (Greiner Bio-one). Two thousand single melanoma cells were plated in triplicate in 2 mL of RPMI supplemented with N2 (Invitrogen) in ultra low attachment 6-well plates (Corning). Breast cancer cell lines were plated similarly in DMEM supplemented with B27 (Invitrogen), hydrocortisone, insulin, rEGF and gentamicin (Lonza). After 5 days, spheres were counted. The number of spheres was divided by the number of cells plated to derive the sphere formation efficiency percentage.

Wound healing assay

To quantify the ability of pathway activators to affect the ability of cells to migrate, 5×10^5 cells were seeded into 6-well plates in triplicate. After 24 hours, the media was changed to growth media containing 1% FBS. The cells were cultured for an additional 24 hours and then evenly wounded. The wound was rinsed twice with PBS and then fresh media containing 1% FBS was added. The wound was photographed at 0 hours and every 12 hours subsequently.

Annexin-V apoptosis assay

To quantify the induction of apoptosis in inhibitor-treated cells, cells were plated in triplicate at 300,000 cells per well in 6-well plates. Twenty-four hours later, cells were treated with the indicated dose of drug or diluent (DMSO). After a 72-hour incubation, cells were washed twice with PBS and resuspended in Annexin V binding buffer composed of 10 mM HEPES, 140 mM NaCl and 2.5 mM $CaCl_2$ (BD Biosciences). Surface exposure of phosphatidylserine was measured using APC-conjugated Annexin V (BD Biosciences). 7-AAD (BD Biosciences) was used to quantify viability. All treatments were evaluated at 20,000 counts/sample using BD FACSVantage SE. Gatings were defined using appropriate untreated/unstained cells.

Statistics

Results are expressed as the means ± SD. For comparisons between two groups, *P*-values were calculated with unpaired, two-tailed Student's *t* tests.

Supplementary Material

Refer to Web version on PubMed Central for supplementary material.

Acknowledgments

We thank Cory Johannessen, Ruwan Gunaratne, Dennie Frederick, Amanda Nichols, Eran Hodis, and Eli Van Allen and the members of the McDonnell, Sabatini, and Wood labs for helpful discussions and technical assistance. This work was supported by Duke University School of Medicine start-up funds and support from the Duke Cancer Institute (K.C.W.), the N.I.H. Building Interdisciplinary Research Careers in Women's Health Program (K.C.W.), a Harry J. Lloyd Trust Translational Research Award (K.C.W.), a Golfers Against Cancer Research Award (K.C.W.), a Stewart Trust Fellowship (K.C.W.), a V Scholar Award from the V Foundation for Cancer Research (K.C.W.), and NIH Grants CA103866 (D.M.S.), AI07389 (D.M.S.), and R37DK048807 (D.P.M.). D.M.S. is an investigator of the Howard Hughes Medical Institute. All cDNA constructs described here have been deposited in Addgene.

References and Notes

1. Glickman MS, Sawyers CL. Converting cancer therapies into cures: lessons from infectious diseases. Cell. 2012; 148:1089. [PubMed: 22424221]
2. Azam M, Latek RR, Daley GQ. Mechanisms of autoinhibition and STI-571/imatinib resistance revealed by mutagenesis of BCR-ABL. Cell. 2003; 112:831. [PubMed: 12654249]
3. Johannessen CM, et al. COT drives resistance to RAF inhibition through MAP kinase pathway reactivation. Nature. 2010; 468:968. [PubMed: 21107320]
4. Engelman JA, et al. MET amplification leads to gefitinib resistance in lung cancer by activating ERBB3 signaling. Science. 2007; 316:1039. [PubMed: 17463250]
5. Straussman R, et al. Tumour micro-environment elicits innate resistance to RAF inhibitors through HGF secretion. Nature. 2012; 487:500. [PubMed: 22763439]

6. Wilson TR, et al. Widespread potential for growth-factor-driven resistance to anticancer kinase inhibitors. Nature. 2012; 487:505. [PubMed: 22763448]
7. Weinberg, RA. The Biology of Cancer. Garland Science; New York: 2007.
8. Yang XP, et al. A public genome-scale lentiviral expression library of human ORFs. Nat Methods. 2011; 8:659. [PubMed: 21706014]
9. Possemato R, et al. Functional genomics reveal that the serine synthesis pathway is essential in breast cancer. Nature. 2011; 476:346. [PubMed: 21760589]
10. Alcala AM, Flaherty KT. BRAF inhibitors for the treatment of metastatic melanoma: clinical trials and mechanisms of resistance. Clin Cancer Res. 2012; 18:33. [PubMed: 22215904]
11. Poulikakos PI, Rosen N. Mutant BRAF melanomas-dependence and resistance. Cancer Cell. 2011; 19:11. [PubMed: 21251612]
12. Gray-Schopfer VC, Karasarides M, Hayward R, Marais R. Tumor necrosis factor-alpha blocks apoptosis in melanoma cells when BRAF signaling is inhibited. Cancer Res. 2007; 67:122. [PubMed: 17210691]
13. Wood KC, et al. MicroSCALE screening reveals genetic modifiers of therapeutic response in melanoma. Sci Signal. 2012; 5:rs4. [PubMed: 22589389]
14. Benjamin CW, Hiebsch RR, Jones DA. Caspase activation in MCF7 cells responding to etoposide treatment. Mol Pharmacol. 1998; 53:446. [PubMed: 9495810]
15. Emery CM, et al. MEK1 mutations confer resistance to MEK and B-RAF inhibition. Proc Natl Acad Sci USA. 2009; 106:20411. [PubMed: 19915144]
16. Flaherty KT, et al. Combined BRAF and MEK inhibition in melanoma with BRAF V600 mutations. New Engl J Med. 2012; 367:1694. [PubMed: 23020132]
17. Ring A, Dowsett M. Mechanisms of tamoxifen resistance. Endocr Relat Cancer. 2004; 11:643. [PubMed: 15613444]
18. Garrett JT, Arteaga CL. Resistance to HER2-directed antibodies and tyrosine kinase inhibitors: mechanisms and clinical implications. Cancer Biol Ther. 2011; 11:793. [PubMed: 21307659]
19. Nickoloff BJ, et al. Jagged-1 mediated activation of notch signaling induces complete maturation of human keratinocytes through NF-kappaB and PPARgamma. Cell Death Differ. 2002; 9:842. [PubMed: 12107827]
20. Kalluri R, Weinberg RA. The basics of epithelial-mesenchymal transition. J Clin Inv. 2009; 119:1420.
21. Wang Z, et al. Targeting Notch signaling pathway to overcome drug resistance for cancer therapy. Biochim Biophys Acta. 2010; 1806:258. [PubMed: 20600632]
22. Muellner MK, et al. A chemical-genetic screen reveals a mechanism of resistance to PI3K inhibitors in cancer. Nat Chem Bio. 2011; 7:787. [PubMed: 21946274]
23. Cho S, et al. Notch1 regulates the expression of the multidrug resistance gene ABCC1/MRP1 in cultured cancer cells. Proc Natl Acad Sci USA. 2011; 108:20778. [PubMed: 22143792]
24. Xie M, et al. Activation of Notch-1 enhances epithelial-mesenchymal transition in gefitinib-acquired resistant lung cancer cells. J Cell Biochem. 2012; 113:1501. [PubMed: 22173954]
25. Rizzo P, et al. Cross-talk between notch and the estrogen receptor in breast cancer suggests novel therapeutic approaches. Cancer Res. 2008; 68:5226. [PubMed: 18593923]
26. Connor CE, et al. Circumventing tamoxifen resistance in breast cancers using antiestrogens that induce unique conformational changes in the estrogen receptor. Cancer Res. 2001; 61:2917. [PubMed: 11306468]
27. Luistro L, et al. Preclinical profile of a potent gamma-secretase inhibitor targeting notch signaling with in vivo efficacy and pharmacodynamic properties. Cancer Res. 2009; 69:7672. [PubMed: 19773430]
28. Loi S, et al. Definition of clinically distinct molecular subtypes in estrogen receptor-positive breast carcinomas through genomic grade. J Clin Oncol. 2007; 25:1239. [PubMed: 17401012]
29. Loi S, et al. Predicting prognosis using molecular profiling in estrogen receptor-positive breast cancer treated with tamoxifen. BMC Genomics. 2008; 9:239. [PubMed: 18498629]

30. Loi S, et al. PIK3CA mutations associated with gene signature of low mTORC1 signaling and better outcomes in estrogen receptor-positive breast cancer. Proc Natl Acad Sci USA. 2010; 107:10208. [PubMed: 20479250]
31. Frederick DT, et al. BRAF inhibition is associated with enhanced melanoma antigen expression and a more favorable tumor microenvironment in patients with metastatic melanoma. Clin Cancer Res. 2013; 19:1225. [PubMed: 23307859]
32. Landsberg J, et al. Melanomas resist T-cell therapy through inflammation-induced reversible dedifferentiation. Nature. 2012; 490:412. [PubMed: 23051752]
33. Engelman JA, et al. Allelic dilution obscures detection of a biologically significant resistance mutation in EGFR-amplified lung cancer. J Clin Inv. 2006; 116:2695.
34. Rizos H, et al. BRAF inhibitor resistance mechanisms in metastatic melanoma: spectrum and clinical impact. Clin Cancer Res. 2014; 20:1965. [PubMed: 24463458]
35. Garraway LA. A Notch for noncoding RNA in melanoma. New Engl J Med. 2014; 370:1950. [PubMed: 24827041]
36. Forloni M, et al. miR-146a promotes the initiation and progression of melanoma by activating Notch signaling. Elife. 2014; 3:e01460. [PubMed: 24550252]
37. Konieczkowski DJ, et al. A melanoma cell state distinction influences sensitivity to MAPK pathway inhibitors. Cancer Discov. 2014; 4:816. [PubMed: 24771846]
38. Lin WM, et al. Modeling genomic diversity and tumor dependency in malignant melanoma. Cancer Res. 2008; 68:664. [PubMed: 18245465]
39. Root DE, Hacohen N, Hahn WC, Lander ES, Sabatini DM. Genome-scale loss-of-function screening with a lentiviral RNAi library. Nat Methods. 2006; 3:715. [PubMed: 16929317]
40. Gupta P, et al. Identification of selective inhibitors of cancer stem cells by high-throughput screening. Cell. 2009; 138:645. [PubMed: 19682730]
41. Dunleavy K, et al. Dose-adjusted EPOCH-rituximab therapy in primary mediastinal B-cell lymphoma. New Engl J Med. 2013; 368:1408. [PubMed: 23574119]
42. Romond EH, et al. Trastuzumab plus adjuvant chemotherapy for operable HER2-positive breast cancer. New Engl J Med. 2005; 353:1673. [PubMed: 16236738]
43. Van Cutsem E, et al. Cetuximab plus irinotecan, fluorouracil, and leucovorin as first-line treatment for metastatic colorectal cancer: updated analysis of overall survival according to tumor KRAS and BRAF mutation status. J Clin Oncol. 2011; 29:2011. [PubMed: 21502544]
44. Cohen MH, Gootenberg J, Keegan P, Pazdur R. FDA drug approval summary: bevacizumab plus FOLFOX4 as second-line treatment of colorectal cancer. Oncologist. 2007; 12:356. [PubMed: 17405901]
45. Ware KE, et al. A mechanism of resistance to gefitinib mediated by cellular reprogramming and the acquisition of an FGF2-FGFR1 autocrine growth loop. Oncogenesis. 2013; 2:e39. [PubMed: 23552882]
46. Guzman C, Bagga M, Kaur A, Westermarck J, Abankwa D. ColonyArea: an ImageJ plugin to automatically quantify colony formation in clonogenic assays. PLoS One. 2014; 9:e92444. [PubMed: 24647355]
47. Perego M, et al. Heterogeneous phenotype of human melanoma cells with in vitro and in vivo features of tumor-initiating cells. J Invest Dermatol. 2010; 130:1877. [PubMed: 20376064]
48. Shaw FL, et al. A detailed mammosphere assay protocol for the quantification of breast stem cell activity. J Mammary Gland Biol Neoplasia. 2012; 17:111. [PubMed: 22665270]

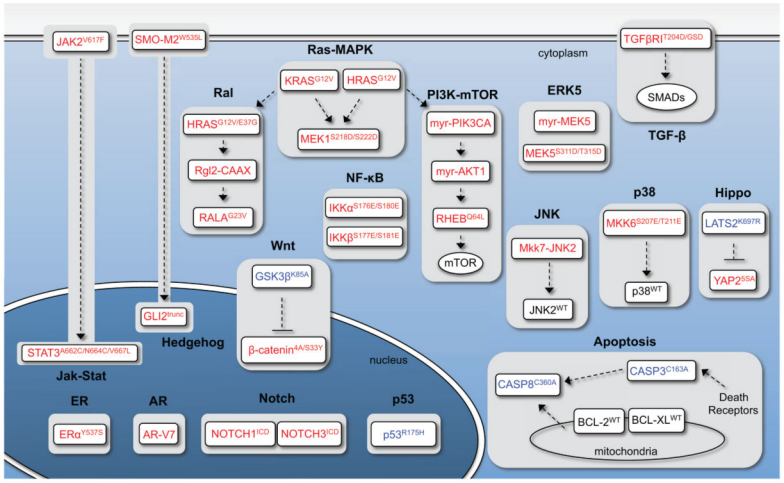

Fig. 1. Strategy for manipulating oncogenic signaling pathways

Pathway names are indicated in bold and situated in the cellular context in which they function. The engineered cDNA constructs in each pathway are denoted as either wild-type (WT; black), constitutively active mutants (red), or dominant-negative mutants (blue).

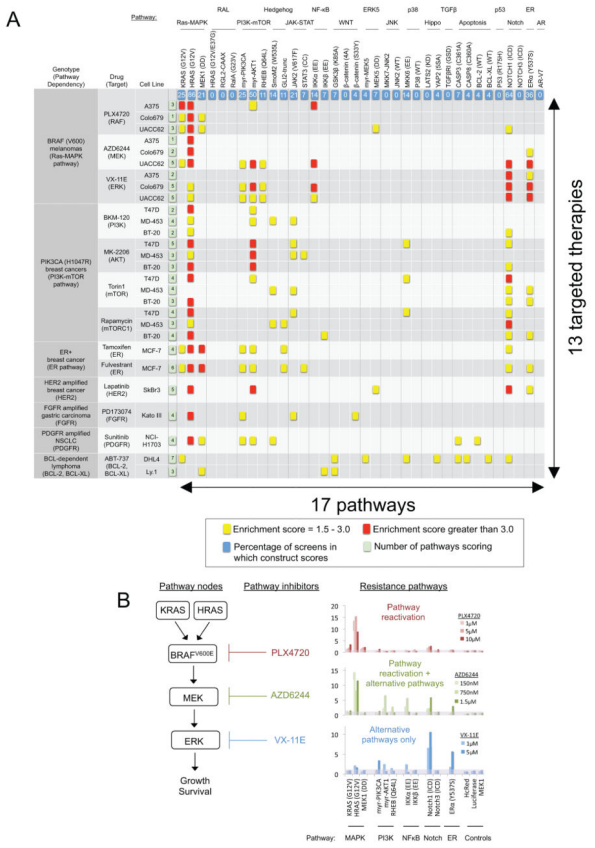

Fig. 2. Global analysis of screening results

(A) Results of each screen color coded according to enrichment score (the relative abundance of each construct in the presence of drug normalized to the same value in the absence of drug). **(B)** Pathway activating constructs scoring in screens involving UACC-62 $BRAF^{V600E}$ melanoma cells treated with PLX4720 (RAF inhibitor, red/top), AZD6244 (MEK inhibitor, green/middle), or VX-11E (ERK inhibitor, blue/bottom).

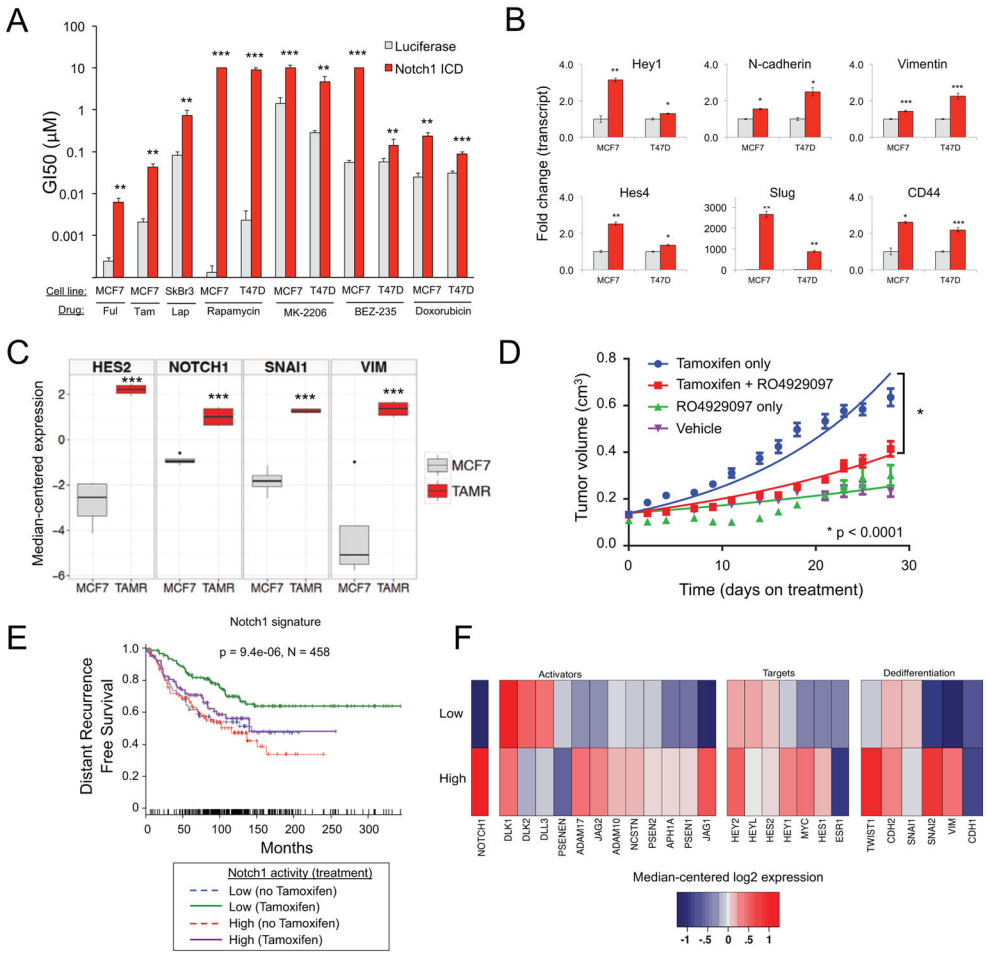

Fig. 3. Notch1 pathway activation confers resistance to targeted therapies in breast cancer, including tamoxifen

(A) GI50 values for indicated breast cancer cell lines expressing Notch1 ICD or luciferase and treated with the indicated drugs. Data are means ± SD from three experiments. **(B)** qRT-PCR analysis of Notch1 target genes and mesenchymal markers in breast cancer cell lines expressing Notch1 ICD (red) or luciferase (gray). Data are means ± SD from three experiments. **(C)** Expression of indicated genes in parental MCF-7 and TamR cells. Data are means ± SD from three experiments. **(D)** Growth of TamR xenografts treated with tamoxifen, RO4929097 (γ-secretase inhibitor), or the combination. Data are means ± SEM from 9–13 mice per group. Exponential growth curve and two-way ANOVA analyses were performed using GraphPad Prism 6. **(E)** Kaplan-Meier plot depicting survival in breast cancer patients treated with tamoxifen as a function of Notch1 pathway gene expression signature level (first and third tertiles). P-value denotes significance between drug treated patients in high and low Notch1 groups. **(F)** Expression heatmap of indicated genes in Notch1 low and high groups from patients in part (E). * $p < 0.1$; ** $p < 0.05$; *** $p < 0.01$

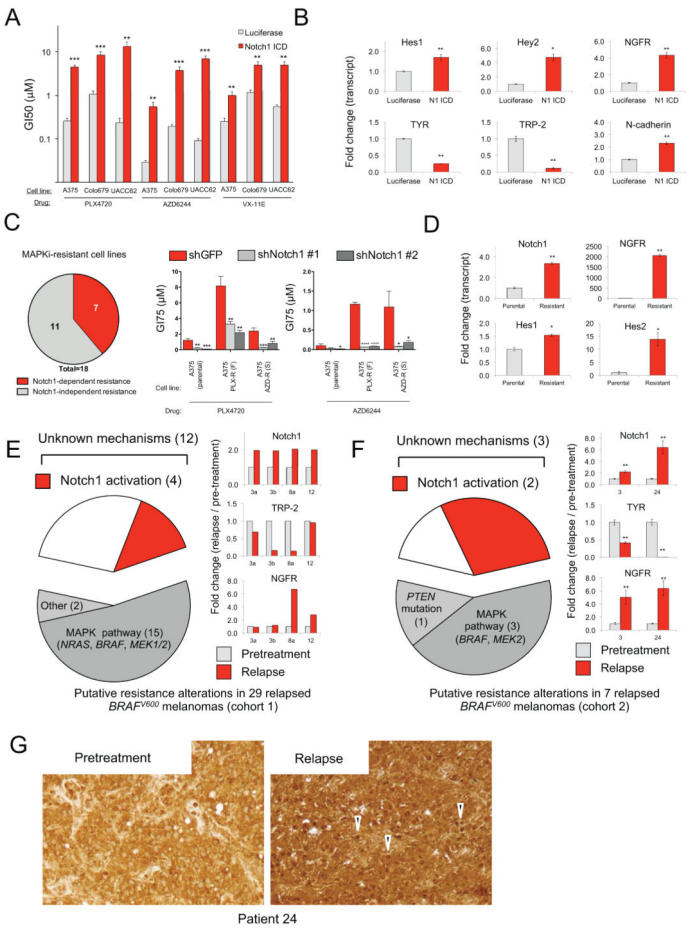

Fig. 4. Notch1 pathway activation in *BRAF*-mutant, MAPK pathway inhibitor-resistant melanoma

(A) GI50 values for indicated melanoma cell lines expressing Notch1 ICD or luciferase and treated with the indicated drugs. Data are means ± SD from three experiments. **(B)** qRT-PCR analysis of Notch1 target genes and differentiation markers in UACC-62 cells expressing Notch1 ICD (red) or luciferase (gray). Data are means ± SD from three experiments. **(C)** Notch1-dependent resistance in cell lines with evolved resistance to MAPK inhibitors (left) as identified by resensitization in the presence of Notch1 knockdown (examples, right). Data are means ± SD from three experiments. **(D)** qRT-PCR analysis of Notch1, Notch1 target genes, and NGFR in Colo679 cells with evolved Notch1-dependent resistance to PLX4720. Data are means ± SD from three experiments. **(E)** Putative mechanisms of resistance in a cohort of 29 relapsed tumors from $BRAF^{V600}$ melanoma patients. “Other” indicates *AKT1* mutation (one patient) or IGF-1 overexpression (one patient). Inset shows fold changes in expression levels of indicated genes on relapse in the Notch1 activation group. **(F)** Putative mechanisms of resistance in a second cohort of seven relapsed tumors from $BRAF^{V600}$ melanoma patients. Inset shows fold changes in expression levels of indicated genes on relapse in the Notch1 activation group. Data are means ± SD from three experiments. **(G)** Analysis of Notch1 nuclear localization by immunohistochemistry in matched pretreatment and relapse samples from Patient 24.

Examples of nuclear Notch1 are indicated by arrowheads. *$p < 0.1$; ** $p < 0.05$; *** $p < 0.01$.

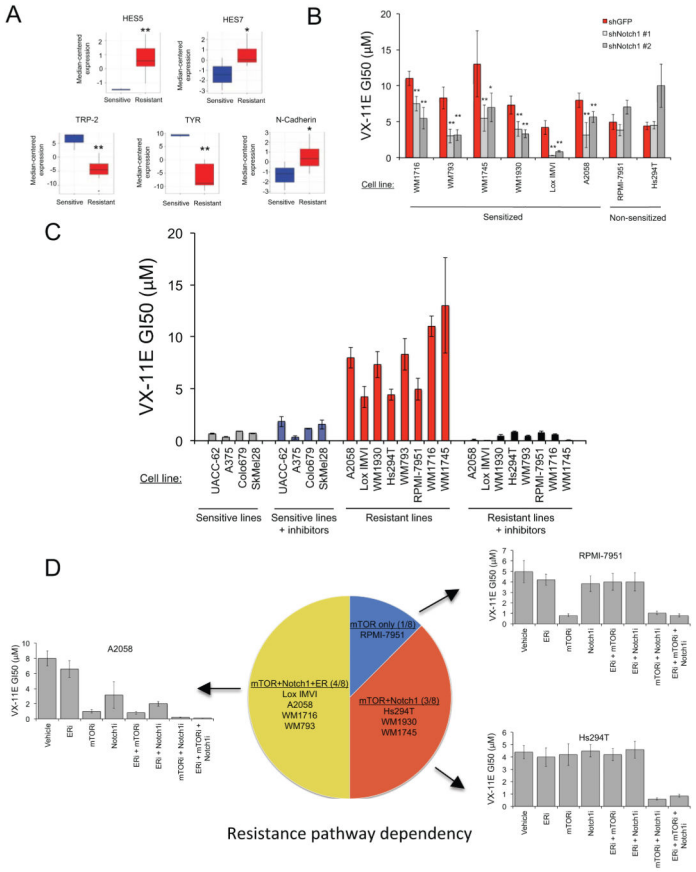

Fig. 5. Simultaneous co-inhibition of multiple drug resistance pathways converts intrinsically drug resistant melanoma cell lines and short-term cultures to a drug sensitive state

(A) qRT-PCR analysis of Notch1 target genes and differentiation markers in MAPK inhibitor–sensitive or intrinsically resistant melanoma cell lines. Data presented are means ± SD from three experiments. **(B)** Effect of shRNA-mediated knockdown of Notch1 on the sensitivity of intrinsically resistant melanoma cell lines to VX-11E. Data are means ± SD from three experiments. **(C)** VX-11E GI50 values measured in *BRAF*-mutant melanoma cell lines and short-term cultures treated with a cocktail of resistance pathway inhibitors (blue, black) or vehicle (gray, red). Resistance pathway inhibitors are shNotch1, BEZ-235 (200 nM), and fulvestrant (1 μM). Data are means ± SD from three experiments. **(D)** Resistance pathway dependencies in drug-resistant cell lines inferred from drug sensitizer assays using all combinations of resistance pathway inhibitors. Data for all GI50 curves are means ± SD from three experiments.